EPJ D
Atomic, Molecular, Optical and Plasma Physics
EPJ.org
your physics journal

Eur. Phys. J. D **54**, 141–148 (2009) DOI: 10.1140/epjd/e2009-00073-1

Microdischarges in ceramic foams and honeycombs

K. Hensel

EDP SCIENCES
Società Italiana di Fisica
Springer

Eur. Phys. J. D **54**, 141–148 (2009)
DOI: 10.1140/epjd/e2009-00073-1

THE EUROPEAN PHYSICAL JOURNAL D

Regular Article

Microdischarges in ceramic foams and honeycombs

K. Hensel[a]

Division of Environmental Physics, Department of Astronomy, Earth Physics and Meteorology,
Faculty of Mathematics, Physics and Informatics, Comenius University, Mlynska Dolina, 842-48 Bratislava, Slovakia

Received 2nd September 2008 / Received in final form 28 January 2009
Published online 6 March 2009 –

Abstract. Microdischarges in spatially confined geometries, such as microcavities and micropores of various materials, present a promising method for the generation and maintenance of stable discharges at atmospheric pressure. They have been successfully used in many biomedical, environmental and industrial applications. The paper presents two relatively new types of discharges in confined volumes – a capillary microdischarge in ceramic foams and a sliding discharge inside the capillaries of ceramic honeycombs – and describes their basic physical properties and mechanisms. Microdischarges inside the microporous ceramic foams develop from the surface barrier discharge if the amplitude of the applied voltage reaches given threshold, but only for a specific pore size. Sliding discharge inside the honeycomb capillaries is produced by a combination of AC barrier discharge inside catalytic pellet bed coupled in series with DC powered honeycomb monolith. Both discharges produce relatively cold microplasmas with high level of non-equilibrium. The basic characteristics of the microdischarges, addressing the effects of the applied voltage, discharge power, pore size, length and diameter of the capillaries are discussed.

PACS. 52.80.-s Electric discharges – 52.75.-d Plasma devices

1 Introduction

Atmospheric pressure non-equilibrium microplasmas are very attractive for their various applications, such as surface modifications, ozone generation, environmental and biomedical processing. The advantage of the microplasmas is that they produce high densities of chemically active species at relatively low energy consumption without any vacuum equipment requirements. The atmospheric microplasmas can be generated by various types of electric discharges, usually dielectric or ferroelectric barrier discharges. They are typical with microdischarges, which form and propagate along the surface of the material and may spread into a wide surface discharge. The microdischarges are filaments of high current density with radius of hundreds μm and duration limited to few ns controlled by charge build up at the dielectric surface. The accumulated charge reduces the electric field to such extent that the current is extinguished. The microdischarges can be generated not only at the surfaces, but also inside spatially confined volumes, e.g. microcavities or micropores of various conductive and insulating materials. A number of such configurations and devices have been developed in the past decade. Among them, probably the most attention has been given to a micro-hollow cathode discharge and a capillary plasma electrode discharge [1].

The micro-hollow cathode discharge (MHCD) [2–4] has become attractive because of its potential to generate high-pressure, non-equilibrium plasmas with no instabilities. The typical device consists of a metallic hollow cathode and an arbitrarily shaped metallic anode separated by an insulator. Under a certain circumstances, determined mostly by the applied voltage, the positive space charge of a glow pre-discharge enters the cathode. There, it acts as a virtual anode and creates a radial electric field. The electric field is responsible for the strong acceleration of the electrons and their oscillatory motion inside the cathode. The electrons undergo many ionizing collisions with the background gas thus creating high-density plasma. Another type of the discharge, which can be generated in a confined geometry, is the capillary plasma electrode discharge (CPED) [4–6]. Electrode design looks similar to a conventional dielectric barrier discharge, but uses dielectric capillaries (diameter of 0.01–1 mm, length-to-diameter ratio of ∼10:1) that cover one or both electrodes. The capillaries serve as plasma sources, which produce jets of high-intensity stable plasma at atmospheric pressure under the right operating conditions (capillary geometry, dielectric material, exciting electric field, etc.). Despite its similarity, the properties of CPED were found distinctly different from those of the dielectric barrier discharge. A configuration similar to CPED employing nano- or microporous dielectric barrier on the electrodes instead of regular capillaries been reported recently [7–9].

[a] e-mail: hensel@fmph.uniba.sk

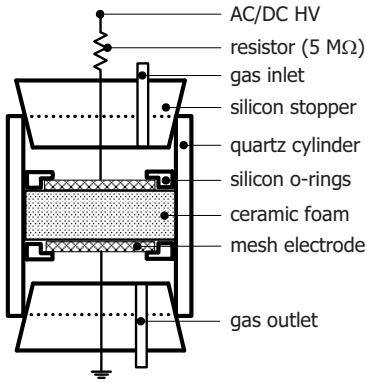

Fig. 1. Reactor for generation of capillary microdischarges in ceramic foams.

The paper introduces two other relatively new configurations for generation of microplasmas in spatially confined volumes and describes the physical properties based on performed electrical and optical measurements. They are: capillary microdischarge in porous ceramic foams and sliding discharge inside honeycomb monolith. The original interest to investigate these discharges has been motivated by the search of a suitable combination of conventional automobile honeycomb catalytic converter by its integration with a non-thermal plasma. It is well-known that integration of catalysts with the plasma results into improved removal efficiency of the exhaust gases, excellent carbon balance, and minimal aerosol production. The process can be effective even at low gas temperature and in oxygen-rich conditions. The generation of the stable plasma inside microcavities, micropores and microchannels of various catalytic materials may therefore represent such an alternative. The paper presents basic electrical and optical characteristics of the microdischarges in ceramic foams and capillaries, addressing the effects of the applied voltage, discharge power, pore size, length and diameter of the capillaries. It also discusses selected applications devoted mainly to the generation or the removal of selected gaseous compounds.

2 Discharges in porous ceramics

Several tests with ceramic foams of various pore size and thickness were performed to unveil the physical properties of microdischarges generated inside the foams by either DC power [10,11] or AC power [12,13]. The ceramic foams had a shape of disks of 31 mm diameter, thickness of 3 and 7 mm and pore size ranging from 2 to 200 μm. They were placed between two mesh electrodes and sealed inside the quartz tube. Simplified sketch of the discharge reactor is depicted in Figure 1.

The formation of microplasmas inside the micropores of ceramic foams was found possible only above the specific discharge voltage determined by the pore size of the ceramics. We found that at a small applied voltage, a barrier discharge developed and was observed on the surfaces of the ceramic foam. Figure 2a shows the typical

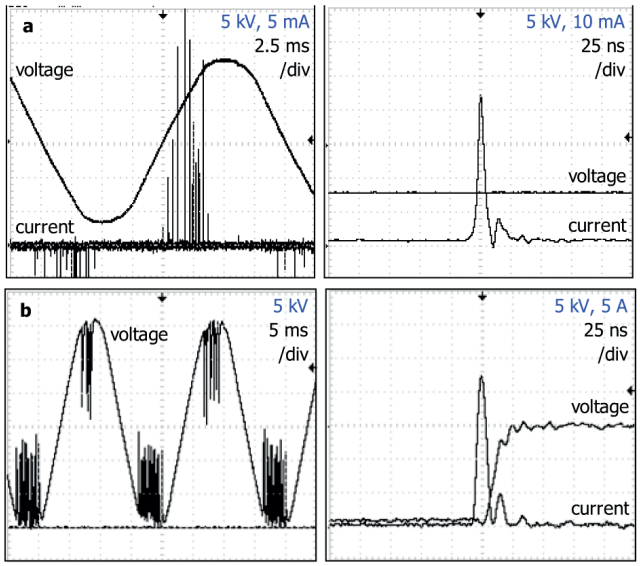

Fig. 2. Voltage and current waveforms of (a) surface barrier discharge ($U_{AC} = 12.2$ kV, $P = 0.1$ W), and (b) capillary microdischarges ($U_{AC} = 16.2$ kV, $P = 6.7$ W) in porous ceramics at two different timescales (pore size 30 μm, air).

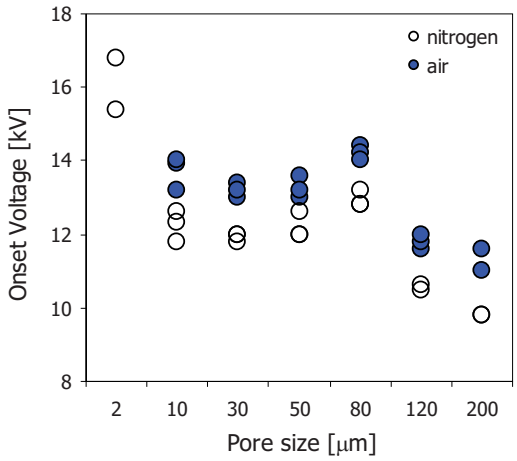

Fig. 3. (Color online) Onset voltage of the capillary microdischarges in nitrogen and air.

waveforms of the applied voltage and the corresponding discharge current of the surface barrier discharge. The discharge current pulses had amplitudes of several tens of mA and were accompanied with insignificant voltage drop. With further increase of the voltage, the surface barrier discharge transits into capillary microdischarges inside the ceramics. The microdischarges inside the ceramics are repetitive discharges, which forms from the foregoing barrier discharge. The onset voltage of the capillary microdischarges was found to increase with the decreasing pore size (Fig. 3). For very small pores (usually less than 2 μm) the onset voltage was too high, therefore mostly the surface discharge was observed here. It was also found that by increasing the thickness of the ceramics by a factor of two, the onset voltage nearly doubled [11]. Upon the transition to capillary microdischarges, the discharge current,

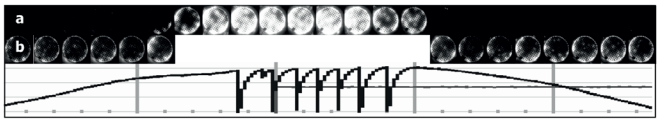

Fig. 4. Discharge emission recorded by ICCD camera and corresponding part of the ac applied high voltage waveform (pore size 80 μm, nitrogen, $U_{AC} = 15.7$ kV, camera gate time 500 μs, camera sensitivity 500 (a), 600 (b), signal integration 100×).

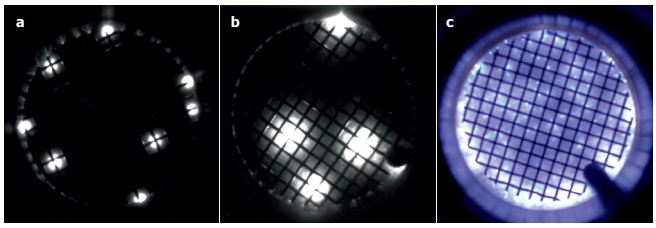

Fig. 5. (Color online) Images of capillary microdischarges as taken by ICCD camera in ceramics of (a) pore size 10 μm, (b) pore size 80 μm (camera gate time 1 ms and sensitivity 420). Image (c) taken by digital camera in 80 μm pore size ceramics (exposure time 1 s, ISO 100, $f/4$). All images were taken in nitrogen, $U_{AC} = 16$ kV.

the amplitude of the current pulses, and corresponding discharge power increased more rapidly with the applied voltage. The microdischarges were accompanied by sharp current pulses with amplitudes reaching several tens of amps and a significant voltage drop (Fig. 2b). The slope of the current-voltage characteristics increased with the pore size, due to an increase of the radius of the discharge channel and volume of the generated microplasma [12]. For the ceramics with pore size bigger than several hundreds of micrometers, no repetitive microdischarges formation was observed. In this case, the ultimate breakdown between the mesh electrodes was observed, which resulted into a formation of a single pulseless glow discharge channel inside the ceramics. This discharge is characteristic by a permanent decrease of the voltage to several kilovolts and significant increase of the mean discharge current to few mA limited only by the ballasting resistor [14].

The transition of the barrier discharge to the capillary microdischarges influenced electrical as well as optical characteristics of the discharge. Figure 4 shows the temporal development of the discharge emission along the ac applied voltage signal recorded by the intensified CCD (ICCD) camera system. In the figure, each image shows the light recorded during the corresponding part of the waveform shown below and integrated in 100 exposition cycles. The figure shows the images with an intense light emission in the region around the maximum amplitude of the applied voltage and substantially smaller intensity in other regions. The emission of the small intensity (noticeable only with higher camera sensitivity) was attributed to the surface barrier discharge, which developed on the surface of the ceramics at low applied voltages. On the other hand, the intensive light emission was attributed to the capillary microdischarges inside the ceramics. The light emission of the microdischarges is much stronger compared to the diffuse homogeneous light of the surface barrier discharge. Synchronizing the electrical and optical characteristics, it was found that each microdischarge in the ceramics was accompanied by a light emission, current pulse and corresponding voltage drop [13].

Figure 5a shows the image for 10 μm pore size ceramics taken by ICCD camera during a period of 1 ms at the maximal amplitude of the applied voltage. The image pattern created by the microdischarges during the specified time period was found different to that observed in the subsequent cycle. It showed that the microdischarges are randomly distributed both in time and space, and the consecutive microdischarges do not occur in the same place. The delay between the repetitive microdischarges was several hundreds of μs and decreased with the amplitude of the applied voltage. Figure 5b is the image of the microdischarges taken in the same conditions as Figure 5a, but in the ceramics with 80 μm pore size. The comparison of the two images shows the diameter of the emission spots increased with the pore size. The diameter of the spot is determined by the diameter of the microdischarge channel and corresponding discharge volume. At a given voltage, the mean discharge current and the amplitude of the current pulses were found higher for 80 μm pore size. Figure 5c shows the image of microdischarges taken by a conventional digital camera with much longer exposure time. The image shows that microdischarges are generated in the whole volume of the ceramics and their distribution is relatively homogeneous. The most intense emission was observed at the sharp edges of the mesh electrode, since the electric field intensity was the highest here. In pure nitrogen, the light emission homogeneously covered the whole ceramics, however with the increase of oxygen and carbon dioxide in the mixture, the discharge homogeneity and thus the light emission distribution deteriorated [12].

The mechanism governing the capillary microdischarges inside the ceramic foams is related to the back-corona phenomenon that occurs when a porous dielectric layer (e.g. dust particles) of high resistivity is present at the electrodes. The layer does not allow charges generated by the discharge to decay, which results in an accumulation of the charges on the layer. When the voltage drop across the layer exceeds a critical value, an ultimate breakdown through the layer occurs. Repetitive charge accumulations and subsequent breakdown of the dielectric layer result in regular repetitive pulsed microdischarges, as we have observed. Generally, the back-corona occurs as a barrier discharge on the dielectric layer, which transforms into microdischarges through the layer. In our case, the layer is represented by the ceramic foam. The transition of the barrier discharge into a capillary microdischarge inside the ceramics is crucial in a way to understand the mechanism of the microdischarges. Considering the geometry and the dimensions of the reactor, the discharge is very similar to MHCD or CPED discharges. The mechanism of MHCD, however, cannot be applied for the ceramics foams, as they are not electrically conductive and

therefore no radial electric field component can form inside the pores. With respect to the geometry of the dielectric barrier between electrodes, the microdischarges are more similar to CPED. The CPED displays two modes of operation – a diffuse mode and a capillary mode – depending on the frequency and the amplitude of the applied voltage. The diffuse mode is similar to the diffuse glow of dielectric barrier discharge, while capillary mode is typical with an intense plasma jet emerging from the capillaries. The transition between the two modes is accompanied by a drastic increase of the electron density and discharge current [1]. Two modes of operation, as well as, the apparent increase of the discharge current upon the transition to capillary microdischarges were also observed with the ceramic foams. The capillary microdischarges inside the microporous foams are spark discharges, whose transition into an arc is avoided by a small energy stored in the capacitor represented by the capacity of the electrodes and connecting cables. It is also prevented by the fact that the current through the capillaries is self-limiting, i.e. the gas density inside the capillary decreases with time due to gas heating [6]. The properties of microdischarges are critically determined by their interaction with the dielectric walls of the capillaries. During the microdischarge, the production of the charged particles is limited by ambipolar diffusion toward the walls of the pores and volume recombination. The ceramics have high thermal shock resistance and effective heat dissipation. The erosion of the ceramics by the microdischarges was found to be very slow, particularly when using AC power supply instead of DC. Using DC power, the charges are accumulated on one surface and the probability of permanent (non-pulsing) breakdown and subsequent mechanical damage of the ceramics is high. An alternative charging and discharging of the ceramics surface by the applied harmonic voltage with AC power is much better and preferable also with respect to applications of the discharges [11,12].

The plasma chemical effects of the capillary microdischarges generated inside porous ceramics have been demonstrated by several papers. They were found effective for ozone generation [15,16] and for exhaust gas cleaning [17]. In pure oxygen, the ozone yield and efficiency were found increasing with the discharge power, but independent of the gas flow rate when energy density was considered. In air-like mixtures, the maximal ozone generation and minimal formation of other by-products was found at low discharge powers and high gas flow rates. The ozone production efficiency increased with the initial concentration of oxygen up to approximately 10% in nitrogen. Due to the negative effect of oxygen on the discharge distribution and homogeneity, with initial concentration of oxygen higher than 10%, the ozone efficiency paradoxically decreased. The capillary microdischarges as spark discharges produced also a limited amount of nitrogen oxides. Their production may become critical with high energy densities. Therefore, these conditions were found not optimal for ozone generation. However, they are assumed to be rather effective for VOC treatment. Loading the ceramics with an appropriate catalyst (e.g. TiO_2), the treatment efficiency is expected to be further improved and formation of undesired by-products suppressed.

There have been a few other works dealing with the discharges generated inside the ceramic foams and their use for various applications. Koo et al. [18,19] used porous ceramics of few hundred micrometers pore size to generate hydrogen in the mixtures of sulfur dioxide and water vapors. The authors tested the effect of the plasma generated by the microdischarges inside the ceramic foams, but also the effect of the electrochemical method employing the ceramic foams with palladium or platinum catalyst coated membrane attached. Although the stability of the microdischarges was quite sensitive to the pore diameter, they found the systems efficient for hydrogen generation. Kraus et al. [20] investigated the discharges generated inside the ceramic foams and used it for CO_2 reforming of methane. In the system, the ceramic foam of 420 μm pore size was placed inside the quartz tube, which separated the ceramics from direct contact with metal electrodes. They found the foam affecting the properties of the generated discharge and significantly increasing the efficiency of the plasma chemical reactions. It was explained with higher average electron energies due to the smaller discharge volumes in the pores of the ceramic foam. The presence of the ceramic foam in the gap was also found to be an effective way to control the temperature in the barrier discharge, with positive influence to product yield.

3 Discharges in honeycomb monolith

Generation of homogeneous and stable atmospheric plasma inside thin and long channels of honeycomb catalysts has been relatively difficult. The discharge in such confined geometry has a relatively high onset voltage compared to the discharge in an open (non-confined) space, due to the losses of charged particle by interaction with the channel walls. The discharge in the capillary is also more unstable with frequent sparking. Another, but more serious, problem of the discharges inside the ceramic honeycombs is that it has been quite difficult to avoid undesirable mechanical breakdowns of the ceramic walls caused by the discharge action. Despite described difficulties, there have been several successful attempts to generate the discharge inside ceramic honeycomb monoliths in the past.

Kim [21] investigated the generation of the discharges inside the capillaries of zeolite-based Co-ZSM-5 honeycomb type catalytic monolith and used it for NOx removal. He powered the honeycomb by a system of wires set inside the channels of the honeycomb (alternatively powered or grounded) or by mesh electrodes set between several smaller blocks of the monolith perpendicularly to the capillaries. Despite promising results for NOx removal, he found the configurations not easy to operate due to frequent sparking, which resulted into ultimate insulation failure of the catalyst. Blin-Simiand et al. [22] and Ayrault et al. [23] generated the discharge inside one-layer honeycomb arrangement (a layer of several channels in a single row) placed between two plate electrodes and

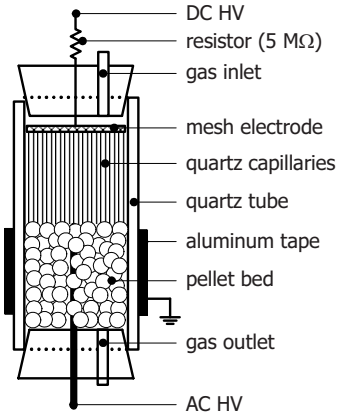

Fig. 6. Reactor for generation of sliding discharge in glass capillaries.

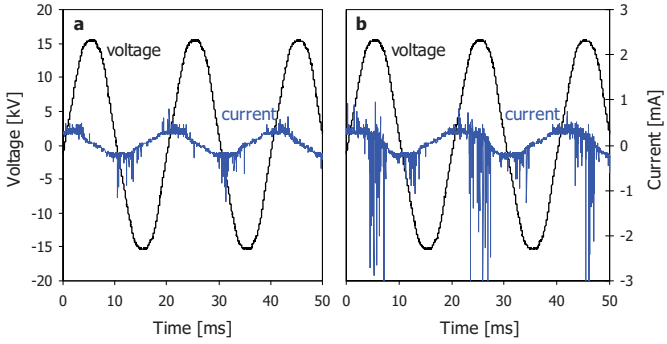

Fig. 7. (Color online) Waveforms of the applied voltage and discharge current of (a) barrier discharge (U_{AC} = 16 kV, U_{DC} = 0 kV) and (b) sliding discharge (U_{AC} = 15 kV, U_{DC} = −16 kV).

investigated the degradation of the odorous compounds by the generated plasma. They found plasma filaments crossing the channels or propagating along the surface and randomly distributed within the honeycomb structure. They also recognized the problem of "hot spots" caused by the streamers drilling holes through the walls.

This paper presents a novel approach of setting up a stable discharge plasma inside honeycomb channels utilizing so-called "sliding discharge". Originally, the sliding discharge has been developed for laser applications [24] and indicated the discharge generated along the dielectric or ferrite surfaces. The discharge on the surface can be generated either between a pair of electrodes in two-electrode system [25,26], or by a combination of AC and DC powers in a three-electrode geometry [27–31]. In the three electrode system, first a barrier discharge is excited locally by AC voltage applied across the dielectric layer. Subsequently, by an application of DC component to the third remote electrode located beyond the dielectric layer, the streamers of the barrier discharge propagate and "slide" along the dielectric surface producing the large-scale surface plasma. Unlike the generation of the sliding discharge on the flat dielectric surfaces, we used the proposed technique to generate the discharge inside the channels of honeycomb monolith, i.e. along the surface of dielectric capillaries [32].

The reactor consisted of a bundle of quartz capillaries with inner diameter of 2 mm, lengths of 2 and 3 cm packed inside the quartz tube of 26 mm diameter and placed on the top of Al_2O_3 pellet bed (Fig. 6). The set of electrodes consisted of stainless steel rod plugged in the middle of the pellet bed, aluminum foil wrapped around the quartz tube and a mesh electrode placed on the top of the capillaries. The rod was powered by AC (50 Hz), the mesh by negative DC high voltage, and the foil was grounded. The bundle of capillaries was used instead of ceramic honeycomb monolith in order to visually observe the discharges inside the channels. The electrical characteristics of the discharges generated in the configurations with the bundle of glass capillaries and with ceramics honeycomb monolith of similar dimensions gave roughly the same results [33]. Therefore, we found the substitution of the honeycomb monolith by a bundle of capillaries acceptable for the subsequent experiments.

The application of the AC power resulted into formation of the streamer discharge plasma inside in the pellet bed. Figure 7a shows the waveforms of both the applied voltage and the current of AC driven packed-bed discharge. The current signal shows the shape typical for a barrier discharge, consisting of a capacitive current envelope with small positive and negative pulses corresponding to the streamer microdischarges. The plasma of the barrier discharge was generated to serve as an ionizing electrode at one end of the capillaries. Upon the application of DC voltage to the mesh electrode at the other end of the capillaries, the streamers propagated into the capillaries and formed the sliding discharge. As a result, stable and homogeneous plasma was produced inside the capillaries. Figure 7b shows the waveform recorded during the operation of the sliding discharge. Compared to the previous figure, negative pulses of much bigger amplitude in the phase with the maximum of the applied voltage can be recognized. These are the pulses of the sliding discharge as measured on the grounded electrode. The pulses were the result of the charge transfer between the electrodes. When negative DC was used, the pulses occurred only in the positive half-cycle of the AC applied voltage. During the positive half-cycle, the positive ions produced in the pellet-bed slided through the capillaries toward the negatively charged mesh electrode. The negative pulses are the image charges of the positive ions collected on the mesh electrode. On the contrary, during the negative half-cycle, it seems no charge was transferred between the two electrodes as they were on the potential of the same polarity.

Figure 8 shows images of the discharges with various AC and DC applied voltages. With only AC or DC voltage applied, the barrier discharge in the pellet bed (Fig. 8b) and the corona discharge in the vicinity of the mesh electrode and above the pellet bed (Fig. 8c) were observed, respectively. The sliding discharge inside the capillaries occurred only if both DC and AC were applied (Fig. 8d). The images also show that the discharge distribution inside

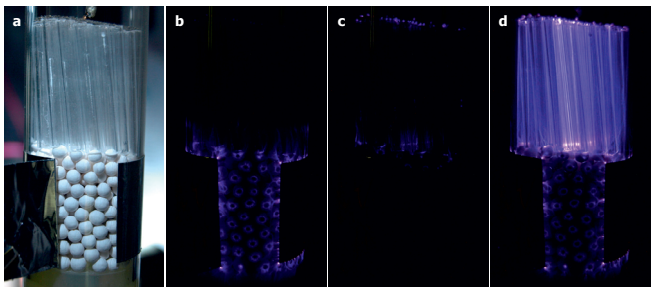

Fig. 8. (Color online) Images of the discharge in capillaries (diameter 2 mm, length 3 mm) at different AC and DC applied voltages in ambient air: (a) the reactor, (b) barrier discharge (U_{AC} = 16 kV, U_{DC} = 0 kV), (c) corona discharge (U_{AC} = 0 kV, U_{DC} = −20 kV), (d) sliding discharge (U_{AC} = 15 kV, U_{DC} = −16 kV).

the capillaries and the light emission along the capillaries were relatively homogeneous. At high amplitudes of the DC applied voltage, sparking occasionally occurred. The transition of the sliding discharge into a spark can be suppressed by ballasting the DC line with the appropriate resistor. Operating the sliding discharge in negative and positive DC polarity showed the applied voltage interval for the stable operation of the sliding discharge without sparking was bigger in the negative polarity [33]. Excessive sparking was also observed when operating in dry gas mixtures. The increase of the humidity in air and nitrogen supported streamer-like behavior of the discharge and suppressed sparking.

Figure 9a shows the power of the sliding discharge as a function of the DC applied voltage for various lengths of the capillaries and amplitudes of AC applied voltage. The discharge power increased with both DC and AC applied voltages and decreased with the length of capillaries. The AC barrier discharge power was one order of magnitude less than that of the DC discharge, therefore its contribution to the total power was negligible. Considering the dimensions of the capillaries, by extending their length at a given DC voltage, the discharge current and power decreased. The diameter of the capillary had, however, only marginal effect on the discharge power [34]. In contrast to negligible effect of AC barrier discharge on the total discharge power, its effect on the discharge emission was found very significant. Figure 9b shows the emission intensity of the sliding discharge based on the spectral band (337 nm) of 2nd positive system of nitrogen as a function of the DC voltage. The intensity increased with both DC and AC applied voltages and the effect of AC voltage on the emission intensity was quite evident. The intensity reflects a concentration of active species generated by the discharge and can be considered as an indirect measure of plasma chemical activity of the discharge. With respect to possible applications, which require maximal yield or efficiency at minimal power consumption it seems appropriate to maximize AC and minimize DC applied voltage to keep the same intensity, i.e. the chemical activity of the discharge. The figure also shows the intensity decreased for longer capillaries, due to a decrease of the corresponding

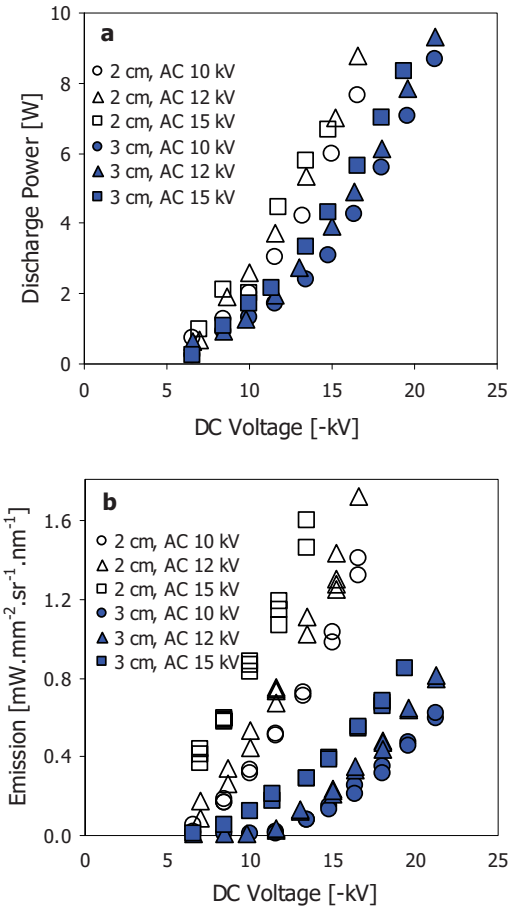

Fig. 9. (Color online) Discharge power (a) and emission intensity (b) as functions of negative DC applied voltage.

discharge current. The analysis of the rotational and vibrational temperatures by simulating the emission spectra using Specair software [35] showed the plasma generated by the sliding discharge was non-equilibrium.

The mechanism governing the sliding discharge is possible to explain by a superposition of the barrier discharge and the DC corona discharge. The first one works as an ionizer, producing charged particles and ionic space charges. The latter one produces and maintains an ionic wind toward the DC electrode. Some of the important data and interpretations of the sliding discharge development and results of the ionic wind measurements can be found in [28,31].

The plasma chemical effects of the sliding discharge have been demonstrated so far only partially. Sato et al. [34] used the sliding discharge for exhaust gas treatment, specifically for the collection of suspended particles and NO oxidation. The efficiency of particle collection was found to significantly improve when gas flow rate increased from 3 to 10 L/min. Occasional sparking, which occurred inside the honeycomb, caused that some particles already trapped were released again, thus resulting into decrease of the efficiency.

4 Conclusions

The paper introduced the two types of discharges for the generation of microplasmas in spatially confided geometries: capillary microdischarge in porous ceramic foams and sliding discharge inside the bundle of capillaries simulating honeycomb monolith. We described the basic physical properties of these microdischarges, based on their electrical and optical characteristics and discussed the possible mechanisms of their formation. Some data of their use in selected applications, especially for exhaust gas treatment, were also presented.

Generation of the microdischarges inside the microporous ceramic foams showed that the pores size and the amplitude of the applied voltage were the critical parameters for their formation. If the pore size and the voltage were small, the surface barrier discharge developed. Above a certain voltage threshold the discharge might break into the ceramics. The transition of the surface barrier discharge into a capillary discharge inside the ceramics is determined by the elementary processes inside the capillaries, mainly by the diffusion of the charged particles and their interaction with the dielectric walls of the capillaries. The microdischarges were distributed randomly both in time and space and homogeneously in the whole volume of the ceramics. The homogeneity of the distribution was found, however, strongly affected by the gas mixture composition. The tests of ozone generation and NOx removal demonstrated the promising plasma-chemical potential of the capillary microdischarges.

Sliding discharge inside honeycomb capillaries was produced by a superposition of AC barrier discharge inside catalytic pellet bed coupled in series with DC powered honeycomb monolith. The streamer plasma formed in the pellet bed served as an ionic electrode. Upon the application of DC field across the capillaries, the streamers propagated into the capillaries forming the plasma inside. The homogeneity and the stability of the plasma were largely dependent on the polarity and ballasting resistor of the DC power and gas mixture humidity. The paper also quotes several tests of the discharges in the honeycombs for NOx, VOC and suspended particle matter removal from diesel exhaust gases.

The atmospheric microplasmas produced by the microdischarges in the presented confined geometries proved their plasma-chemical potential when used in various applications, namely those directed on exhaust treatment. Their potential is expected to further improve when combined in a plasma-catalytic system.

The paper owes much to discussions with and experimental results from staff, students and visitors in the laboratory in Bratislava: Z. Machala, M. Janda, V. Martisovits and M. Lestinsky (Comenius University, Bratislava, Slovakia); S. Sato and A. Mizuno (Toyohashi University of Technology, Japan); P. Tardiveau and S. Pasquiers (Université Paris-Sud, Orsay, France). This research has been supported by the APVT 20-032404, SK-FR-00506 and VEGA 1/3041/06 grants.

References

1. K.H. Becker, K.H. Schoenbach, J.G. Eden, J. Phys. D: Appl. Phys. **39**, R55 (2006)
2. K.H. Schoenbach, R. Verhappen, T. Tessnow, F.E. Peterkin, W.W. Byszewski, Appl. Phys. Lett. **68**, 13 (1996)
3. H.I. Park, T.I. Lee, K.W. Park, H.K. Baika, Appl. Phys. Lett. **82**, 3191 (2003)
4. P. Kurunczi, N. Abramzon, M. Figus, K. Becker, Acta Phys. Slovaca **54**, 115 (2004)
5. A.D. Koutsospyros, S.M. Yin, C. Christodoulatos, K. Becker, IEEE Trans. Plasma Sci. **33**, 42 (2005)
6. N.S. Panikov, S. Paduraru, R. Crowe, P.J. Ricatto, C. Christodoulatos, K. Becker, IEEE Trans. Plasma Sci. **30**, 1424 (2002)
7. J.H. Cho, I.G. Koo, M.Y. Choi, W.M. Lee, Appl. Phys. Lett. **92**, 101504 (2008)
8. S.J. Park, J.G. Eden, IEEE Trans. Plasma Sci. **33**, 572 (2005)
9. T. Kawasaki, Y. Nakayama, T. Yamauchi, IEEE Trans. Plasma Sci. **38**, 1324 (2008)
10. K. Hensel, Y. Matsui, S. Katsura, A. Mizuno, Czech. J. Phys. **54**, C683 (2004)
11. K. Hensel, S. Katsura, A. Mizuno, IEEE Trans. Plasma Sci. **33**, 574 (2005)
12. K. Hensel, V. Martisovits, Z. Machala, M. Janda, M. Lestinsky, P. Tardiveau, A. Mizuno, Plasma Process. Polym. **4**, 682 (2007)
13. K. Hensel, P. Tardiveau, IEEE Trans. Plasma Sci. **36**, 980 (2008)
14. Z. Machala, E. Marode, C.O. Laux, C.H. Kruger, J. Adv. Oxid. Technol. **7**, 133 (2004)
15. M. Lestinsky, K. Hensel, V. Martisovits, in *Proceedings of 16th Symposium on Applications of Plasma Processes (SAPP XVI)*, Podbanske, Slovakia (2007), p. 217
16. K. Hensel, M. Lestinsky, Z. Machala, P. Tardiveau, in *Proceedings of 11th International Symposium on High Pressure Low Temperature Plasma Chemistry (Hakone XI)*, Oléron, France (2008) CD-ROM
17. J. Sawada, Y. Matsui, K. Hensel, I. Koyamoto, K. Takashima, S. Katsura, A. Mizuno, in *Recent Development in Applied Electrostatics*, edited by S. Keping, Y. Gefei (Elsevier, 2004), p. 128
18. I.G. Koo, W.M. Lee, Electrochem. Commun. **9**, 2325 (2007)
19. I.G. Koo, M.Y. Choi, J.H. Kim, J.H. Cho, W.M. Lee, Jpn J. Appl. Phys. **47**, 4705 (2008)
20. M. Kraus, B. Eliasson, U. Kogelschatz, A. Wokaun, Chem. Phys. Chem. **3**, 29 (2001)
21. H.H. Kim, in *Application of Non-thermal Plasma in Environmental Protection*, Ph.D. Thesis, Toyohashi University of Technology, Toyohashi, Japan (2000)
22. N. Blin-Simiand, P. Tardiveau, A. Risacher, F. Jorand, S. Pasquiers, Plasma Process. Polym. **2**, 256 (2005)
23. C. Ayrault, J. Barrault, N. Blin-Simiand, F. Jorand, S. Pasquiers, A. Rousseau, J.M. Tatibouët, Catal. Today **89**, 75 (2004)
24. G.N. Tsikrikas, A.A. Serafetinides, J. Phys. D: Appl. Phys. **9**, 2806 (1996)
25. S.N. Tskhai, D.A. Akimov, S.V. Mitko, V.N. Ochkin, A.Yu. Serdyuchenko, D.A. Sidorov-Biryukov, D.V. Sinyaev, A.M. Zheltikov, J. Raman Spectrosc. **32**, 177 (2001)

26. K.K. Trusov, J. Phys. D: Appl. Phys. **39**, 335 (2006)
27. C. Louste, G. Artana, E. Moreau, G. Touchard, J. Electrostat. **63**, 615 (2005)
28. E. Moreau, C. Louste, G. Artana, M. Forte, G. Touchard, Plasma Process. Polym. **3**, 697 (2006)
29. R. Sosa, H. Kelly, D. Grondona, A. Marquez, V. Lago, G. Artana, J. Phys. D: Appl. Phys. **41**, 035202 (2008)
30. E. Moreau, C. Louste, G. Touchard, J. Electrostat. **66**, 107 (2008)
31. E. Moreau, R. Sosa, G. Artana, J. Phys. D: Appl. Phys. **41**, 115204 (2008)
32. K. Hensel, S. Sato, A. Mizuno, IEEE Trans. Plasma Sci. **36**, 1282 (2008)
33. S. Sato, H. Yamauchi, K. Takashima, A. Mizuno, in *Proceedings of 28th International Conference on Phenomena in Ionized Gases (ICPIG XXVIII)*, Prague, Czech Republic, (2007), p. 1338
34. S. Sato, K. Hensel, H. Yamauchi, K. Takashima, A. Mizuno, in *Proceedings of 31st Annual Meeting of Institute of Electrostatics of Japan*, Tsukuba, Japan (2007), p. 1
35. C.O. Laux, T.G. Spence, C.H. Kruger R.N. Zare, Plasma Sources Sci. Technol. **12**, 125 (2003)